Novel and simplified implementation of digital high-power pulsed MIG welding power supply with LLC resonant converter

Kaiyuan Wu, Hao Huang, Ziwei Chen, Min Zeng and Tong Yin
School of Mechanical and Automotive Engineering, South China University of Technology, Guangzhou, China

Abstract

Purpose – This paper aims to overcome the limitations of low efficiency, low power density and strong electromagnetic interference (EMI) of the existing pulsed melt inert gas (MIG) welding power supply. So a novel and simplified implementation of digital high-power pulsed MIG welding power supply with LLC resonant converter is proposed in this work.

Design/methodology/approach – A simple parallel full-bridge LLC resonant converter structure is used to design the digital power supply with high welding current, low arc voltage, high open-circuit voltage and a wide range of arc loads, by effectively exploiting the variable load and high-power applications of LLC resonant converter.

Findings – The efficiency of each converter can reach up to 92.3%, under the rated operating condition. Notably, with proposed scheme, a short-circuit current mutation of 300 A can stabilize at 60 A within 8 ms. Furthermore, the pulsed MIG welding test shows that a stable welding process with 280 A peak current can be realized and a well-formed weld bead can be obtained, thereby verifying the feasibility of LLC resonant converter for pulsed MIG welding power supply.

Originality/value – The high efficiency, high power density and weak EMI of LLC resonant converter are conducive to the further optimization of pulsed MIG welding power supply. Consequently, a high performance welding power supply is implemented by taking adequate advantages of LLC resonant converter, which can provide equipment support for exploring better pulsed MIG welding processes.

Keywords Power supply, Pulsed MIG welding, Full-bridge LLC resonant converter, Parallel connection, Digital

Paper type Research paper

1. Introduction

Pulsed melt inert gas (MIG) welding corresponds to a high-quality welding method and is widely used in high-performance automatic welding tasks, owing to its characteristics of excellent direction transition, less material splash and desired welding appearance, with a wide welding current adjustment range and excellent capabilities of thin plate, thick plate and all-position welding. Besides, it can control the arc energy, conveniently and accurately. Due to these benefits, it has become one of the most commonly used metal material processing methods (Praveen *et al.*, 2005; Palani and Murugan, 2006; Ghosh, 2017). Additionally, the power supply plays a vital role in defining the overall performance of pulsed MIG welding (Choi *et al.*, 2016; Narula *et al.*, 2016a; Mvola *et al.*, 2018).

The switching mode power supply applied in the welding field generally adopts the inverter topology, which has the development trend focusing on high efficiency, high frequency and digitization (Pang and Zhang, 2010; Yun *et al.*, 2021). Alternatively, to realize the desired output voltage and current control, the high-power pulsed MIG welding power supply is generally based on the full-bridge topology (Wang *et al.*, 2011; Wang and Wu, 2015), where the pulse width modulation (PWM) is used as a control method for conventional hard-switching or soft-switching with phase-shifted full-bridge (PSFB).

However, in the conventional hard-switching circuit with PWM control, the voltage and current of power device overlap each other when the power device is switching, thus resulting in switching loss and low efficiency, which in turn inhibits the increase of switching frequency and restrains the miniaturization of the power supply (Shin, 2016). At the same time, there exists a heavy switching stress to the power device due to the hard-switching state, causing high du/dt and di/dt, which result in strong electromagnetic interference (EMI) and electromagnetic pollution (Narula *et al.*, 2016b). Therefore, it is necessary to design a buffer absorption circuit for the power device, which in return increases the circuit complexity.

Funding: This work was supported by the National Natural Science Foundation of China (Grant No. 51205136), the Basic and Applied Basic Research Foundation of Guangdong Province (Grant No. 2021A1515010678, 2022A1515010255), the Competitive Allocation Project Special Fund of Guangdong Province Chinese Academy of Sciences Comprehensive Strategic Cooperation (Grant No. 2013B091500082), the Fundamental Research Funds for the Central Universities (Key Program) (Grant No. 2015ZZ084), the Science and Technology Planning Project of Guangzhou (Grant No. 201604016015) and the China Scholarship Council (Grant No. 201606155058).

Received 14 March 2022
Revised 30 July 2022
Accepted 10 September 2022

The current issue and full text archive of this journal is available on Emerald Insight at: **https://www.emerald.com/insight/0305-6120.htm**

Circuit World
50/1 (2024) 54–66
 [ISSN 0305-6120]
[DOI 10.1108/CW-03-2022-0068]

In the PSFB circuit with PWM control, for the primary-side metal-oxide-semiconductor field-effect transistor (MOSFET), the realization of zero-voltage switching (ZVS) uses the leakage inductance of transformer and phase-shift control by which the current lags the voltage. PSFB possesses a wide voltage adjustment range and can achieve high power (Hallworth *et al.*, 2013; Aksoy, 2015). However, there exists a bottleneck challenge of achieving ZVS of the lagging bridge under light load. Besides, zero-current switching (ZCS) cannot be realized in the secondary-side rectifier diode, inherently causing the voltage ringing phenomenon and reverse recovery loss. The addition of a buffer absorption circuit is therefore essential to the secondary-side rectifier diode, too (Cho *et al.*, 1996). In the heavy load, excessive current on the primary side aggravates the secondary-side duty loss and the voltage ringing phenomenon. Hence, the primary-side energy cannot be fully transmitted to the secondary side, thereby indicating an increased energy loss and significant reduction in the efficiency of the power supply (Ruan and Yan, 2001; Tran *et al.*, 2018).

Accordingly, the LLC resonant converter and its derivative structure have replaced the above-mentioned topology gradually and have now become an ideal topology choice for designing power supply in some areas, due to their high power density and efficiency (Yang, 2003).

The ZVS on the primary-side MOSFET and the ZCS on the secondary-side rectifier diode can be realized simultaneously for the LLC resonant converter when the operating conditions and load conditions are appropriate. The relevant EMI is weak, and the reverse recovery loss can be avoided. Thus, a considerably high efficiency can be obtained with such topology. Simultaneously, the need for filter inductance at secondary side can be eliminated. Besides, the resonant inductance can also be replaced by the transformer leakage inductance, which can optimize the magnetic components, thus decreasing the production expense and increasing the power density, significantly (Yang *et al.*, 2002). The design of filter and high-frequency transformer becomes easier, because of the high switching frequency with narrow adjustment range, which contributes in alleviating the EMI caused by the reduced size of welding power supply and the increase of switching frequency (Ji *et al.*, 2017). In addition, due to substantial increase in the switching frequency, the volume of the inductor and the transformer reduces dramatically. This minifies the converter volume, increases the converter output capacity per unit volume and further improves the power density.

At present, the research and application of LLC resonant converter are generally concentrated for low and medium power supplies (Mishima *et al.*, 2017; Wu *et al.*, 2017; Li *et al.*, 2018; Li *et al.*, 2019), where load and output are basically constant or vary insignificantly (Narli *et al.*, 2019; Khoshsaadat *et al.*, 2020), such as television. power supply (Demirel and Erkmen, 2014), communication power supply (Watanabe and Kurokawa, 2015), electric vehicle charger (Vu and Choi, 2018) and photovoltaic battery (Tayebi *et al.*, 2020). The LLC resonant converter has been applied quite sophisticatedly in these fields. However, in high-power power supplies, for example, the welding power supply, the ratio of voltage and current, namely, the equivalent resistance of the arc, actually show a drastic variation (Rossi *et al.*, 2016). Therefore, in the welding field, the application of LLC resonant converter is hindered by these restrictions. Nevertheless, if the welding power supply can use the LLC resonant converter, it can significantly enhance the efficiency, minify the converter volume and reduce the EMI.

Currently, for welding power supply applications, resonant converter topologies have attracted the attention of many researchers. Chaouch *et al.* (2021) proposed a model representing the current-output PSFB LCLC resonant converter in arc welding application, which can be applied either in constant voltage characteristic or dropped characteristic welding machines to fulfill either ZCS or ZVS, depending on the switching frequency. Progressively, Kar *et al.* (2021) proposed an efficient SiC-based harmonic-current-assisted LCC load-resonant converter for the arc welding application. The efficiency of converter was further increased by ensuring the ZVS operation of switching devices, irrespective of the load variations. Additionally, the reported converter possessed an inherent short-circuit current limiting capability, which minimizes the control requirement and increases the ruggedness. Wang *et al.* (2019) presented an 8 kW LLC resonant converter particularly designed for the plasma power supply based on SiC power devices, which was lighter in weight, more compact and more efficient than previous designs. Wu *et al.* (2021) proposed a direct-current gas metal arc welding (GMAW) power supply using a parallel full-bridge LLC resonant converter, which realized stable and efficient direct-current GMAW near the theoretical optimal operating point, with 210 A output current.

Although these studies report different specific topologies, they all use the resonant soft-switching for welding applications. Hence, it can be concluded that a resonant converter topology effectively improves the efficiency, due to the soft-switching condition. In addition, there also exist other advantages in using resonant converter topology, including smaller inductor and transformer and weaker EMI. Similarly, our proposed power supply based on LLC resonant converter demonstrates relatively high efficiency and magnetic component integration.

However, the power switch of the LLC resonant converter is a MOSFET. Due to the limitation of switching power device and magnetic material of transformer, the output current of a single LLC resonant converter is low, which is not enough to meet the high current requirement for efficient welding. To overcome this, a high current of 280 A is realized through several parallel LLC resonant converters, whereas the traditional hard-switching or PSFB circuit can realize a similar high current by using just a single converter.

Furthermore, the research on pulsed welding power supply using LLC resonant converter has not been given proper attention yet. Its in-depth research will have a great significance in the advancement of welding power supply and welding technology.

Correspondingly, in this paper, a novel and simplified implementation of digital high-power pulsed MIG welding power supply with LLC resonant converter is proposed. In accordance with the characteristics of pulsed MIG welding, a digital power supply with high welding current, low arc voltage, high open-circuit voltage and a wide range of arc loads, is designed, and its feasibility for pulsed welding is verified. Additionally, multiple parallel modules are connected to adapt the high-power needs. The high efficiency, high power density and weak EMI of LLC resonant converter are conducive to further optimization of pulsed MIG welding power supply.

Consequently, a high performance welding power supply is implemented by taking adequate advantages of LLC resonant converter, which can provide equipment support for exploring better pulsed MIG welding processes.

2. Design of pulsed melt inert gas welding power supply

2.1 Structure of power supply

The main parameters of the pulsed MIG welding power supply are presented in Table 1.

As indicated in Table 1, the power of the power supply reaches 9 kW at the peak stage. Besides, the switching power devices are MOSFETs. Due to the limitation of switching power device and magnetic material of transformer, it is challenging for a single LLC resonant converter to meet the demands for high-power with safety and stability. However, using multiple LLC resonant converters in parallel can not only easily satisfy the high-power requirements of the welding power supply but also distribute the total output power to each converter uniformly, thus highlighting that the output power of each converter is reduced relatively.

At the base stage, the power drops to less than 2 kW. If the total output power is still uniformly distributed to each converter, it will not merely cause a waste of hardware resources, but also the gain of a single converter will be too small. It will lead the switching frequency to a value much higher than the resonant frequency, thereby causing excessive energy loss in the secondary-side rectifier diode and reducing the energy transfer efficiency. Eventually, it will limit the converter advantages.

Therefore, so as to meet the high-power requirements and minimize the limitation on inherent converter advantages, a hardware and software-based power supply solution with a novel and simplified implementation is proposed in this paper. Namely, multiple parallel LLC resonant converters are connected, where one of them is used as base module alone, while the remaining converters are used as peak module. The base current is outputted, when the base module is on and the peak module is off. Likewise, the peak current is outputted, when the peak module is on and the base module is off. By repeating this process, the base and peak modules work alternately, according to the pulse frequency. Figure 1 shows the relevant structure.

Because the base voltage is lower than the rated voltage of LLC resonant converter at the base stage, the switching frequency will be higher than the resonant frequency, which will allow ZVS to be realized on the primary-side MOSFETs, while ZCS will not be realized on the secondary-side rectifier diodes. This consequently will cause a certain amount of power loss.

Table 1 Power supply parameters

Parameter	Value
Input voltage V_{ina} (V)	220 ± 10% (50 Hz)
Open-circuit voltage V_{oc} (V)	55–70
Base current I_b (A)	70–100
Peak current I_p (A)	200–300
Pulse frequency f (Hz)	50–100
Pulse duty D (%)	30–50

Similarly, at the peak stage, the output voltage and current coming from four parallel LLC resonant converters of the peak module are approximately same as the rated voltage and current. Therefore, LLC resonant converter will operate at the resonant frequency. Correspondingly, the best energy transfer efficiency can be achieved.

2.2 Design of control system

Figure 2 is a block diagram of the digital control system for the power supply.

An ARM chip STM32F103RBT6 from STMicroelectronics is used as the core control chip. The control of the power supply is realized by using a software program. In addition, the peak and base modules are connected to each other through the controller area network (CAN) bus. The command information of the CAN bus is updated according to the pulse sequence, to enable a simple implementation of the output switching of the base and peak modules.

Progressively, Figure 3 is the schematic diagram describing the switching of each module and the pulsed current. At the peak stage, the CAN bus command is that the peak module is on and the base module is off. Then, all LLC resonant converters of the peak module operate at the same time to output the peak current, while the base module is turned off without any output, for the duration t_p. Alternatively, at the base stage, the CAN bus command is updated to turn the peak module off and the base module on. Here, the LLC resonant converter of the base module operates alone to output the base current, while the peak module is off without any output, for the duration t_b. The process is repeated continuously to output the pulsed current.

Using this simple control strategy, the output current is kept constant for each LLC resonant converter, which then acts as a virtual constant current (CC) source that works periodically. In this way, the design process is simplified when designing the LLC resonant converter. Moreover, it is possible to ensure that each LLC resonant converter operates near the optimal operating point of the resonant frequency. Thus, the EMI and switching losses are reduced. Similarly, the power supply is more stable and more reliable. Herein, the power devices and magnetic devices are used optimally, and the efficiency of power supply is improved.

2.3 Design of LLC resonant tank

Figure 4 shows the main circuit diagram of the LLC resonant converter.

Table 2 lists the rated operating parameters of the LLC resonant converter, which are used as the basis for designing the parameters of LLC resonant tank.

In this work, the LLC resonant tank is designed using the first harmonic approximation method (Duerbaum, 1998).

Taking the grid voltage fluctuation into consideration, the maximum input voltage V_{ind_max} = 370 V; the rated input voltage V_{ind_rated} = 300 V; the minimum input voltage V_{ind_min} = 250 V. Meanwhile, the rated output voltage and current are V_o = 29 V, I_o = 70 A.

The transformer ratio n is as follows:

$$n = \frac{V_{ind\_rated}}{V_o + V_d} = 10 \quad (1)$$

where V_d is the forward voltage drop of the secondary-side rectifier diode.

Figure 1 Hardware structure diagram of digital high-power pulsed MIG welding power supply

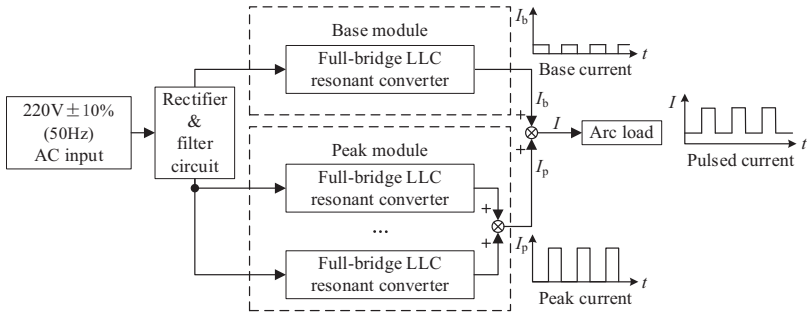

Figure 2 Block diagram of the digital control system

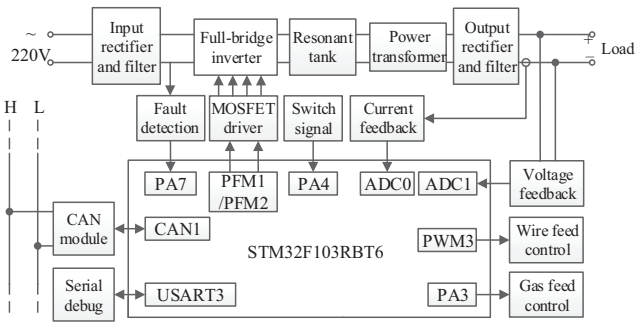

Figure 3 Schematic diagram describing the switching of each module and the pulsed current

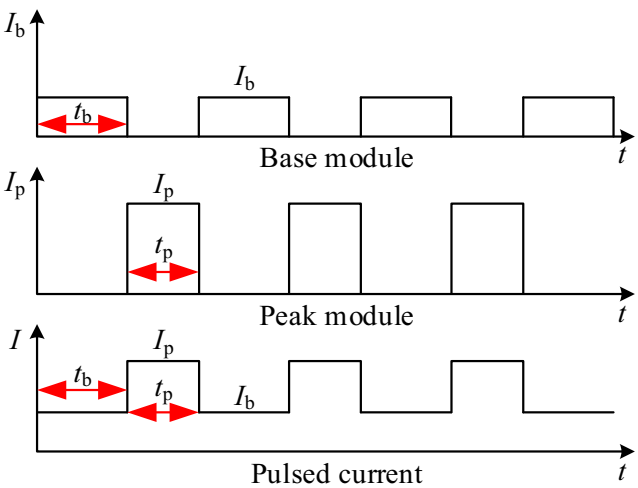

The minimum and maximum voltage gains, respectively, are as follows:

$$G_{\min} = \frac{n \cdot (V_o + V_d)}{V_{ind\_max}} = 0.811 \quad (2)$$

$$G_{\max} = \frac{n \cdot (V_o + V_d)}{V_{ind\_min}} = 1.200 \quad (3)$$

The load equivalent resistance R_L and the equivalent resistance R_e that is converted from the secondary side to the primary side, respectively, are as follows:

$$R_L = \frac{V_o}{I_o} = 0.414\,\Omega \quad (4)$$

$$R_e = \frac{8n^2 R_L}{\pi^2} = 33.6\,\Omega \quad (5)$$

The key strategy for LLC resonant tank design is to find an optimal value of the ratio of magnetizing inductance L_m to resonant inductance L_r, namely, the inductance ratio k. Considering the light-load efficiency of power supply, for one thing, it is essential to lower the turn-off current of the primary and secondary windings effectively; for another, it is indispensable to decrease the operating frequency range of the resonant tank. Hence, owing to this trade-off, $k = 3$ is selected, and the quality factor Q is as follows:

$$Q = \frac{0.95}{k \cdot G_{\max}} \cdot \sqrt{k + \frac{G_{\max}^2}{G_{\max}^2 - 1}} = 0.661 \quad (6)$$

The resonant frequency is selected as $f_r = 80\,\text{kHz}$, and therefore, the minimum switching frequency is as follows:

$$f_{\min} = \frac{f_r}{\sqrt{1 + k\left(1 - \frac{1}{G_{\max}^2}\right)}} = 57.7\,\text{kHz} \quad (7)$$

Furthermore, the maximum switching frequency is as follows:

$$f_{\max} = \frac{f_r}{\sqrt{1 + k\left(1 - \frac{1}{G_{\min}}\right)}} = 145.9\,\text{kHz} \quad (8)$$

Here, to avoid excessive current from damaging the device during short-circuit ignition process, the switching frequency is modified to 65–300 kHz.

The resonant inductor L_r, magnetizing inductor L_m and resonant capacitor C_r, respectively, are as follows:

$$L_r = \frac{Q \cdot R_e}{2\pi f_r} = 44\,\mu\text{H} \quad (9)$$

$$L_m = k \cdot L_r = 133\,\mu\text{H} \quad (10)$$

$$C_r = \frac{1}{2\pi \cdot f_r \cdot R_e \cdot Q} = 89\text{nF} \quad (11)$$

Besides, the ripple current of the secondary output capacitor is as follows:

Figure 4 Main circuit diagram of LLC resonant converter

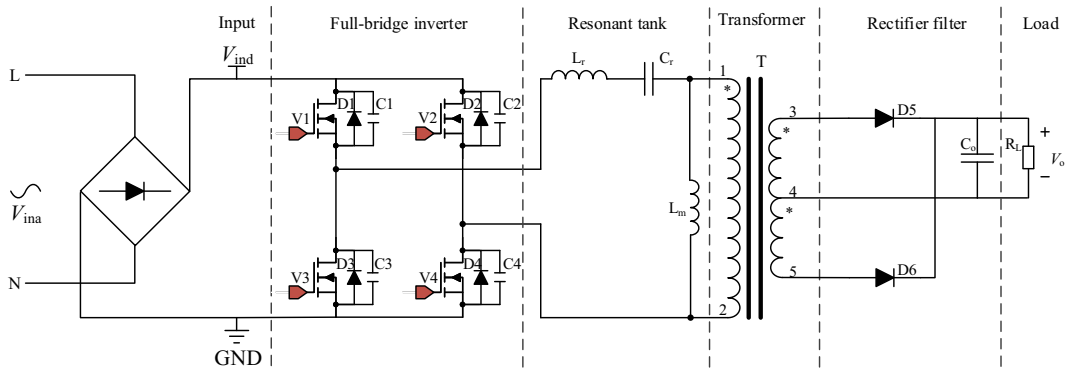

Table 2 Rated operating parameters of the LLC resonant converter

Parameter	Value
Input voltage V_{ina} (V)	220 V ± 10% (50 Hz)
Resonant frequency f_r (kHz)	80
Rated voltage V_o (V)	29
Rated current I_o (A)	70
Transformer turns ratio n	10

$$I_{c_{rms}} = \sqrt{\frac{\pi^2 - 8}{8}} I_o = 33.8\,\text{A} \tag{12}$$

It is assumed that the ripple voltage of the secondary output capacitor is 1% of the rated output voltage, and this ripple voltage is mainly caused by the ripple current flowing through the internal equivalent series resistance R_{esr} of the output capacitor. Then, the ripple voltage is given as:

$$V_{pp} = 0.01 \times V_o = 0.29\,\text{V} \tag{13}$$

In addition, the $R_{esr} \times C_o$ of aluminum electrolytic capacitors with different capacitance levels is constant, about 65×10^{-6} ΩF. Then, the output capacitance is as follows:

$$C_o = \frac{65 \times 10^{-6}\Omega\text{F}}{R_{esr}} = \frac{65 \times 10^{-6}\Omega\text{F}}{V_{pp}/I_{c_{rms}}} = 7558\mu\text{F} \tag{14}$$

To keep enough margin for output capacitance, three aluminum electrolytic capacitors of 3900 μF are connected in parallel.

Table 3 presents the designed parameters.

3. Experimental procedure

3.1 Experimental setup of simulated load test

Figure 5 illustrates the simulated load test platform of LLC high-power pulsed MIG welding power supply.

As shown in Figure 5(a), according to the characteristics of wide-range arc load and wide-range grid voltage fluctuation during the welding process, the performance test of LLC resonant converter under the variable load and input voltage conditions is first carried out. Specifically, for the input voltage V_{ina} of 190 V, 200 V, 210 V, 220 V and 230 V, the corresponding input and output power (P_{in} and P_o) are measured, where the simulated load R_L is 0.2 Ω, 0.3 Ω, 0.4 Ω, 0.5 Ω and 0.6 Ω, respectively. Additionally, the voltage at the mid-point of inverter bridges V_H and the secondary-side current at the center tap of transformer i_s are recorded. The converter efficiency η is calculated using P_{in} and P_o, while the reverse recovery rate of the secondary-side rectifier diode ξ is calculated using V_H and i_s.

The equation for calculating ξ is given as follows:

$$\xi = \frac{1}{N}\sum_{i=1}^{N}\frac{\delta}{I_{max}} \tag{15}$$

where δ is the reverse recovery current, I_{max} is the secondary-side current amplitude and N is the sample size. The larger the ξ, the more serious the reverse recovery phenomenon, the worse the switching condition, the more the energy loss and the more the deviation from the theoretical ideal situation.

Next, the closed-loop test is conducted for a single LLC resonant converter with a CC output, to verify its stability. A digital oscilloscope (TPS2024B, Tektronix, USA) is used to acquire the voltage at the mid-point of the inverter bridges V_H, the primary-side resonant current i_r and the secondary-side current at the center tap of transformer i_s. The experimental condition states that the bus input voltage V_{ind} varies from

Table 3 Designed parameters of the LLC resonant converter

Parameter	Value
Input voltage V_{ina} (V)	220 V ± 10% (50 Hz)
Open-circuit voltage V_{oc} (V)	55–70
Rated voltage V_o (V)	29
Rated current I_o (A)	70
Resonant frequency f_r (kHz)	80
Switching frequency f_s (kHz)	65–300
Resonant inductor L_r (μH)	44
Magnetizing inductor L_m (μH)	133
Resonant capacitor C_r (nF)	89
Output capacitor C_o (μF)	3900 × 3
Primary-side MOSFET	IXFH60N50P3
Secondary-side rectifier diode	DPG60C200HB

Notes: L_r does not include the transformer leakage inductance and uses an external inductor

Figure 5 Simulated load test platform

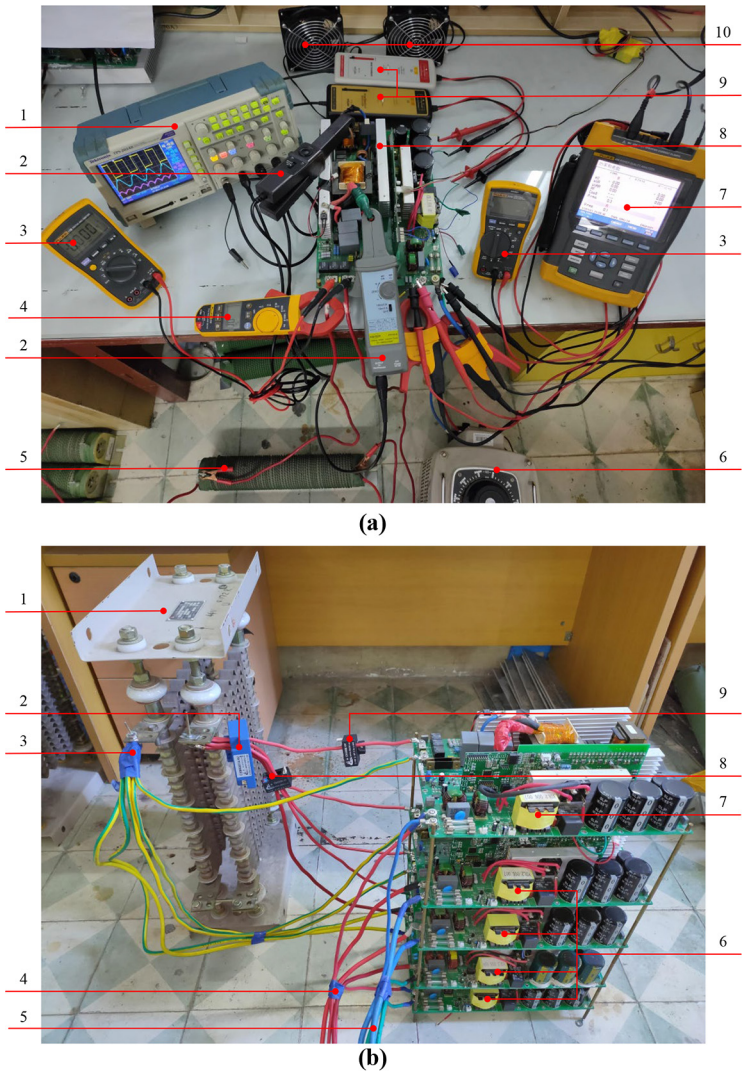

Notes: (a) Performance, closed-loop and short-circuit test of the LLC resonant converter. 1 – Digital oscilloscope; 2 – Current probe; 3 –Digital multimeter; 4 – True-RMS clamp meter; 5 – Load; 6 – Contact voltage regulator; 7 – Power quality analyzer; 8 – LLC power module; 9 – Voltage probe; 10 –Cooling fan; (b) simulated welding test. 1 –Resistance load; 2 –Output pulsed current positive; 3 –Output pulsed current negative; 4 –Input AC live line; 5 –Input AC neutral line; 6 – Peak module; 7 – Base module; 8 –Output of peak module; 9 –Output of base module

240 V to 360 V, the output current is set to 70 A, and the simulated load is the rated load of 0.4 Ω. The simulated load is composed of three 1.2 Ω/3 kW high-power resistors connected in parallel. Meanwhile, for the primary-side MOSFET, the voltage V_{DS} between the drain and source and the voltage V_{GS} between the gate and source are measured to validate the ZVS.

Because the dynamic response of the power supply plays a vital role in determining the welding quality, it is highly essential for the power supply to exhibit outstanding dynamic characteristics. In addition, because the welding power supply adopts the short-circuit striking method, to avoid excessive current from blowing up the machine, it is necessary to perform a short-circuit test on the LLC resonant converter. Factually, the actual welding circuit is not a theoretical short-circuit during the arc striking process; instead, there exists a very small resistance due to the wire and the base metal. Therefore, a resistance of 0.1 Ω is selected to simulate the short circuit. The input is 220 V AC from the grid, and the relevant output voltage and current waveforms are measured.

Furthermore, a simulated welding test is carried out under the rated input and rated load to verify the feasibility of the proposed power supply solution, as shown in Figure 5(b). The output voltage and current waveforms of the peak and base modules are acquired using a digital oscilloscope (DPO2024B,

Tektronix, USA). The welding power supply is composed of five LLC resonant converters. Among them, one is used as the base module, while others are connected in parallel serving as the peak module. The operating conditions for all LLC resonant converters of the peak module are theoretically the same. Set values for the base current I_b = 60 A; the peak current I_p = 240 A; the pulse frequency f = 50 Hz; and the pulse duty D = 40%. The simulated load resistance is selected as 0.172 Ω.

3.2 Experimental setup of pulsed melt inert gas welding test

Direct current electrode positive is used for the power supply. The workpiece is connected to the negative pole, and the filler wire is connected to the positive pole. Accordingly, the voltage and current waveforms are acquired using a digital oscilloscope (DPO2024B, Tektronix, USA).

The base metal is a 600 mm × 50 mm × 4 mm AA6061 aluminum plate. The ER4043 with a diameter of 1.2 mm is used as filler wire to deposit bead on-plate welding.

Table 4 presents the chemical compositions of the base metal and filler wire, while Table 5 lists the welding parameters.

Table 5 Welding parameters

Parameter	Value
Ar shielding gas (%)	99.999
Gas flow rate (L/min)	20
Base current I_b (A)	70
Peak current I_p (A)	280
Pulse frequency f (Hz)	50
Pulse duty D (%)	40
Wire feed speed (WFS) (mm/s)	88
Travel speed (cm/min)	85
Contact tip-to-work distance (CTWD) (mm)	18

4. Results and discussion

4.1 Simulated load test

4.1.1 Performance of LLC resonant converter

Figure 6 shows a diagram displaying the converter efficiency η and the switching frequency f_s, under different loads and input voltages. Similarly, Figure 7 demonstrates the reverse recovery rate of the secondary-side rectifier diode ξ and the switching frequency f_s, under various loads and input voltages. Meanwhile, under closed-loop control, the output current is maintained at 70 A.

As evident from Figures 6 and 7, when the load is heavy, the LLC resonant converter operates in the ZVS zone, the ξ exceeds 80% and the ZCS is not realized for the secondary-side rectifier diode. Simultaneously, the f_s is much higher than the resonant frequency f_r of 80 kHz, thereby reflecting a low efficiency. Alternatively, under the rated load of 0.4 Ω, the f_s approaches the f_r, and the ξ is reduced significantly. At this stage, the η reaches the maximum value. The η is as high as 92.3%, under the rated operating condition of 210 V/0.4 Ω. Moreover, the η can be even higher, if there is no diode full-bridge rectifier present in front of the LLC converter. Progressively, when the load is light, the LLC resonant converter operates in the ZVS-ZCS zone. The ξ is approximately 0, which mitigates a certain amount of energy loss. However, at the same time, the f_s in this case is much lower than the f_r; thus, the η is lower than the optimal.

In case of different input voltages, the η basically increases with the increase of input voltage, and similarly, the ξ also increases with the input voltage. When the input voltage varies from 190 V to 230 V, the corresponding change in η is no more than 3%, which highlights that the grid voltage fluctuation has an insignificant effect on the designed converter efficiency. Notably, both the η and ξ are primarily determined by the load.

4.1.2 Closed-loop test

The measured waveforms of the closed-loop test are shown in Figure 8.

As shown in Figure 8, the resonant current i_r waveform of primary-side in Figure 8(a) has a platform with a switching frequency f_s of 74 kHz. Likewise, in Figure 8(b), the i_r is similar to the 80 kHz sine wave. In Figure 8(c), the resonant current waveform of primary-side experiences a sudden change after the switching signal is switched, and the corresponding f_s is 97 kHz. This shows that under closed-loop control, the f_s can be regulated to operate in the $f_s < f_r$ zone (i.e. the ZVS-ZCS zone), when the bus input voltage V_{ind} is lower than the bus rated voltage. On the contrary, when the V_{ind} is higher than the bus rated voltage, the f_s can be regulated to operate in the $f_s > f_r$ zone, indicating the ZVS zone. Furthermore, when the V_{ind} is at the bus rated voltage, the f_s can be regulated to operate at the resonant frequency.

As indicated through the experimental results, even when the power grid fluctuates in a wide range (i.e. the V_{ind} deviates significantly from the bus rated voltage), the LLC resonant converter can adjust the f_s in real time through the digital closed-loop control system, to adjust the gain and maintain a CC output.

The waveforms of V_{DS} and V_{GS} are shown in Figure 9, under the rated operating conditions. V_{DS} reduces to zero before V_{GS} is turned on, which proves that the primary-side MOSFET realizes the ZVS.

4.1.3 Short-circuit test

The short-circuit test results are plotted in Figure 10. Channels 1 and 2 are output voltage V_o and current I_o waveforms of the power supply, respectively.

It can be seen from Figure 10 that there is no current output when the converter is under the open-circuit condition. Meanwhile, the open-circuit voltage V_{oc} is 56 V, which matches the requirement of arc ignition voltage. Conversely, for the

Table 4 Chemical compositions of base metal and filler wire (Wt.%)

Elements	Mg	Fe	Si	Zn	Cu	Mn	Ti	Cr	Al
AA6061	0.8–1.2	0.7	0.4–0.8	0.25	0.15–0.4	0.15	0.15	0.04–0.35	Bal.
ER4043	≤ 0.05	≤ 0.80	4.5 – 6.0	≤ 0.10	≤ 0.30	≤ 0.05	≤ 0.20	–	Bal.

Figure 6 Efficiency η and switching frequency fs, under different loads and input voltages

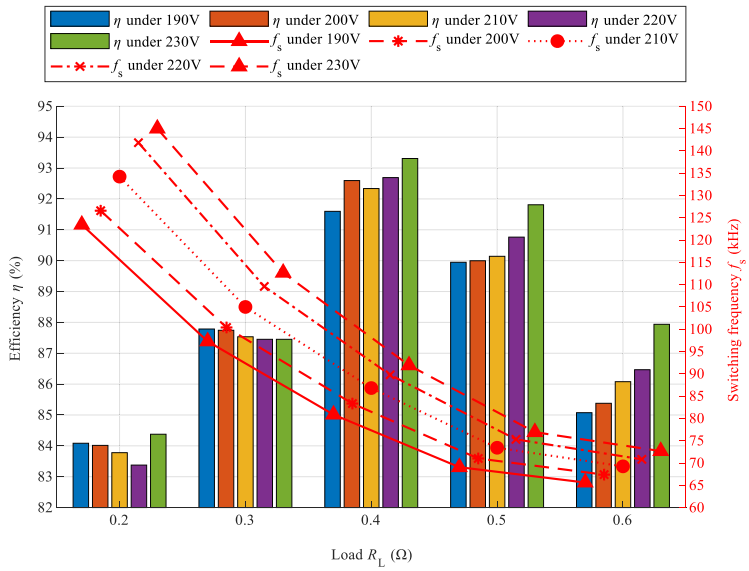

Figure 7 Reverse recovery rate of secondary-side rectifier diode ξ and switching frequency fs, under different loads and input voltages

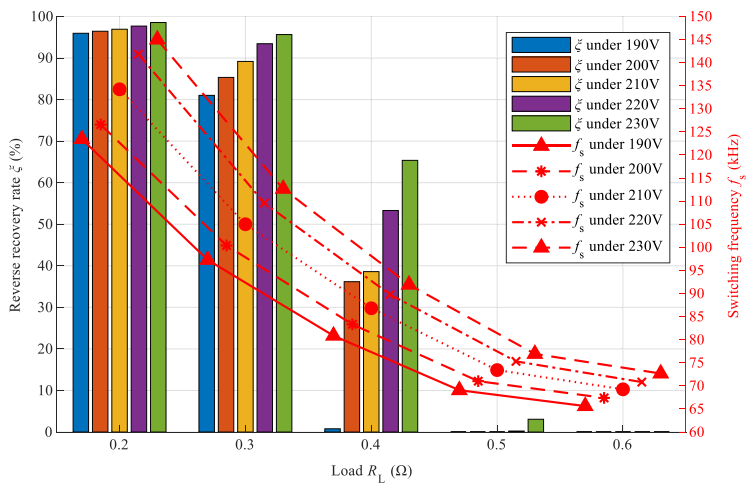

short-circuit condition, the voltage suddenly drops to 7 V, while the current abruptly rises to 60 A. This sudden variation stabilizes within 8 ms, which proves that the rapidity and accurateness of the designed PI closed-loop control algorithm fulfill the relevant requirements. Simultaneously, it is noticed that the output current overshoot rises up to 300 A; however, the overcurrent protection is not triggered during the whole process, and the components of LLC resonant converter are also intact. Besides, it is shown from the waveform that the LLC resonant converter still has a certain output after the switching is completed, and there is no shutdown.

4.1.4 Simulated welding test

To test the output waveforms of the base and peak modules, the base module is connected to a 0.3 Ω load resistor, while the peak module is connected to a 0.1 Ω load resistor. The corresponding results are presented in Figure 11. Channels 1 and 3 are the output voltage waveforms of the peak and base modules, respectively, while channels 2 and 4 are the output current waveforms of the peak and base modules, respectively.

From Figure 11, the output current of the base module is 70 A, while that of the peak module is up to 240 A. This verifies the feasibility of generating the pulse with the proposed pulsed MIG power supply.

Additionally, Figure 12 displays the output waveforms during the simulated arc striking process of the power supply.

The extracted output waveforms from the simulated load test are shown in Figure 13.

It can be seen from Figure 13 that the pulse frequency is 50 Hz, the pulse duty is 40%, the peak current is constant at about 230 A and the base current is constant at 60 A, which is slightly lower than the set value of 240 A. The lower peak current may be because the arc characteristic of the base stage is different from that of the peak stage during the welding process,

Figure 8 Waveforms of the closed-loop test

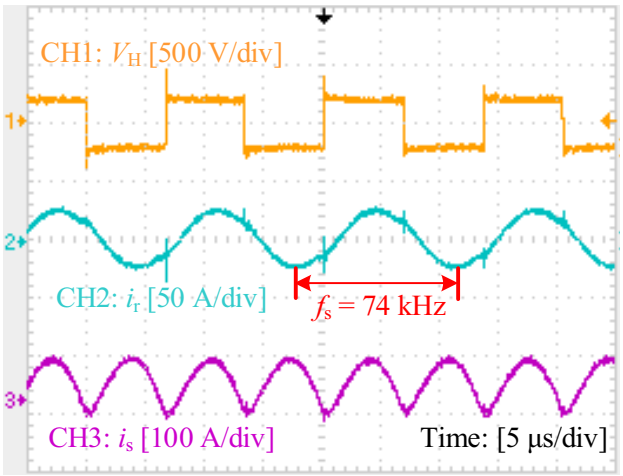

(a)

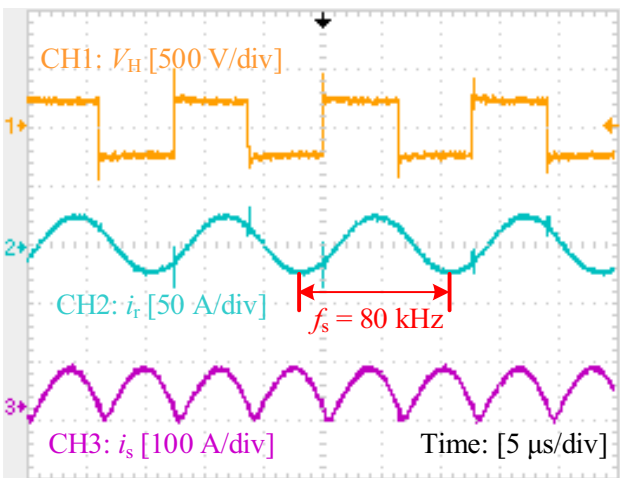

(b)

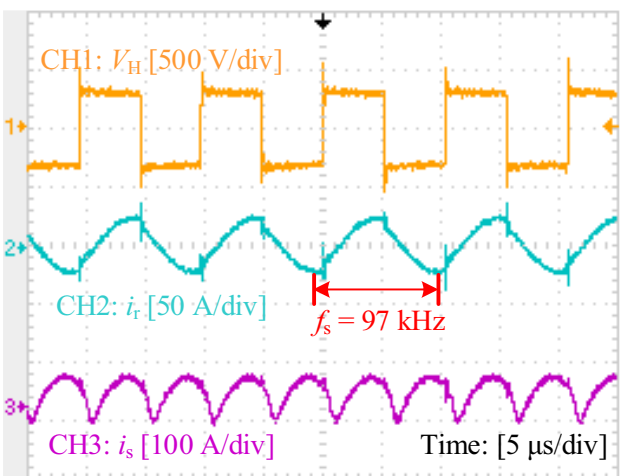

(c)

Notes: (a) V_{ind} = 240 V, R_L = 0.4 Ω; (b) V_{ind} = 295 V, R_L = 0.4 Ω; (c) V_{ind} = 330 V, R_L = 0.4 Ω

Figure 9 DS inter-polar voltage and GS driving voltage waveforms

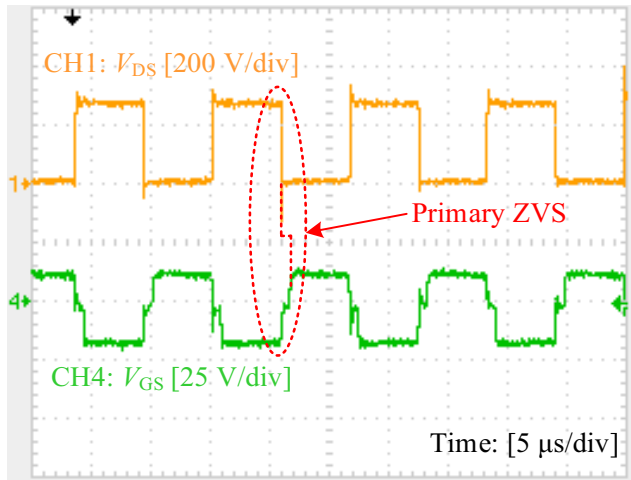

which consequently results in the difference in equivalent resistance. That is to say, the pulsed welding is a process of constantly changing load; nevertheless, the simulated load test here assumes a fixed load, which causes inconsistency between the equivalent load of the base stage and that of the peak stage. Furthermore, it also results in inconsistent operating conditions. In addition, the lower peak current may also be caused by the difference of analog to digital converter sampling circuit on the digital control system. Additionally, the current waveform here is not an ideal square wave. On one hand, it exhibits a ramped rise and fall process with very short duration, which is consistent with the actual circuit situation. On the other hand, there is no obvious overshoot, back groove or tail, which matches the proposed design. Hence, this further verifies the feasibility of generating pulse with the proposed pulsed MIG power supply.

Figure 14 shows the waveforms during the simulated arc extinguishing process.

In summary, a conclusion can be drawn from the results of the simulated load test that the designed pulsed MIG welding power supply can achieve steady and rapid digital control in the arc striking, pulse output and arc extinguishing processes. This verifies the feasibility of both hardware and software control schemes and demonstrates that such schemes can control the welding system precisely and generate the pulsed current stably.

4.2 Pulsed melt inert gas welding test

4.2.1 Welding waveforms

Figure 15 presents the output waveforms during the welding process. Channels 1 and 2 correspond to voltage and current, respectively.

It can be seen from Figure 15 that the output waveforms are consistent with the proposed design. The base current is 70 A; the peak current is 280 A, and the pulse frequency is 50 Hz. The welding process here possesses fine stability without any short-circuit or arc interruption phenomena. Noticeably, the base and peak voltages are about 21 V and 30 V, respectively, compared to the rated output voltage of 29 V. This manifests

Figure 10 Output waveforms of short-circuit test

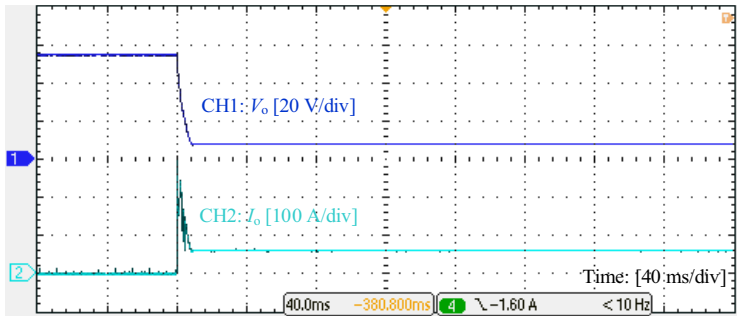

Figure 11 Output waveforms of base module and peak module

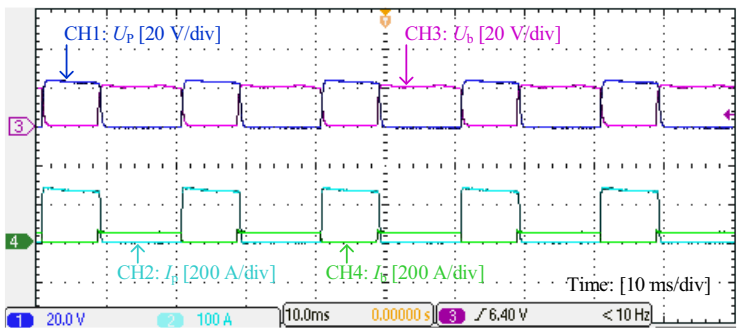

Figure 12 Output waveforms of the arc ignition process of the simulated load test

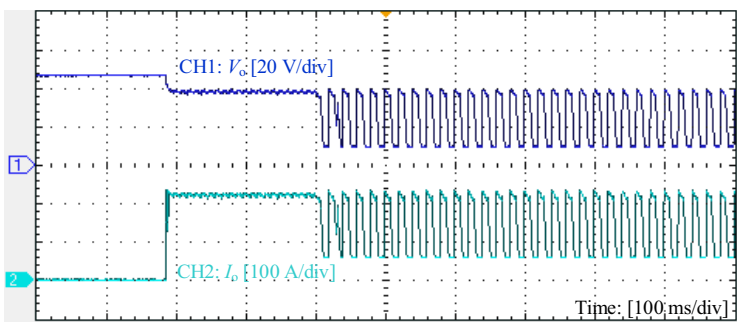

Figure 13 Output waveforms of the simulated load test

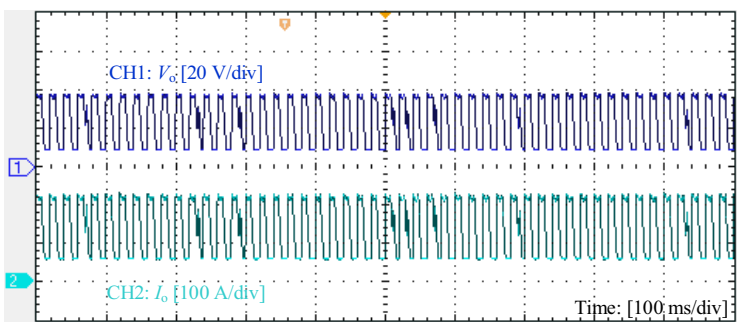

Figure 14 Output waveforms of the arc extinguishing process of the simulated load test

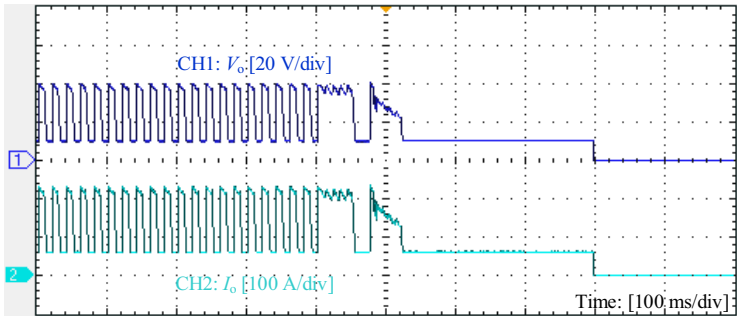

that all LLC resonant converters of the peak module operate approximately at the resonant frequency, while the switching frequency of the base module slightly deviates from the resonant frequency. Overall, a high energy transfer efficiency is achieved, which is consistent with the proposed design.

4.2.2 Weld bead

Figure 16 shows the weld bead gained from the pulsed MIG welding test, which is well formed and has obvious fish scales.

Finally, the welding test results demonstrate that the proposed digital high-power pulsed MIG welding power supply with LLC resonant converter can realize a stable pulsed MIG welding of aluminum alloys. This claim is further validated by obtaining a desired well-formed weld bead. Moreover, there exist obvious fish scales on the weld bead, which verifies the feasibility of LLC resonant converter used for the pulsed MIG welding power supply.

5. Conclusions

A novel and simplified implementation of digital high-power pulsed MIG welding power supply with LLC resonant converter is proposed in this paper. The simulated load test and pulsed MIG welding test are conducted. The main conclusions are as follows:

- The welding power supply structure with base and peak modules working alternately can not only maximize the high-efficiency advantages of the LLC resonant converter, providing an efficiency of 92.3% under rated operating conditions, but also effectively increase the power (the peak current is 280 A).
- The LLC resonant converter can maintain an efficiency of more than 84%, when the load changes from 0.2 Ω to 0.6 Ω and the input voltage varies from 190 V to 230 V,

Figure 15 Welding voltage and current waveforms

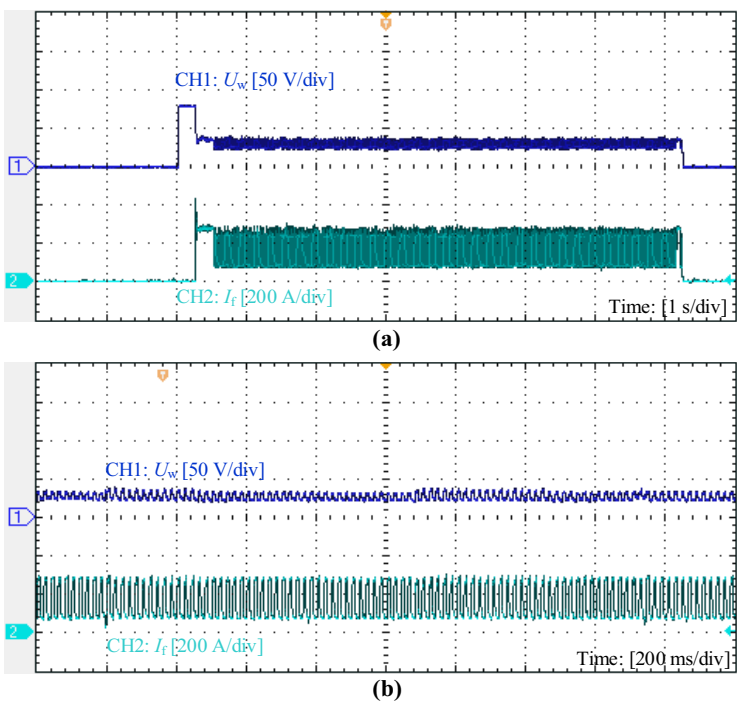

Notes: (a) Macroscopic waveforms; (b) expanded waveforms

Figure 16 Photograph of weld bead

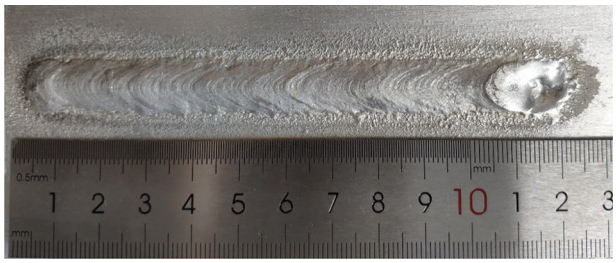

which indicates an excellent stability. Moreover, the grid voltage fluctuation has little effect on the efficiency. Moreover, both the efficiency and the reverse recovery rate of the secondary-side rectifier diode are mainly determined by the load.

- The power supply can quickly adjust the current and voltage in case of short-circuit arc striking, thus demonstrating satisfactory dynamic characteristics.
- The pulsed MIG welding power supply can realize the stable welding of aluminum alloy, and accordingly, a well-formed weld bead is obtained in this work. From the comparison of rated output voltage and arc voltage, it is illustrated that the switching frequency of the peak module is much closer to the resonant frequency, compared to the switching frequency of the base module.

References

Aksoy, I. (2015), "A new PSFB converter-based inverter arc welding machine with high power density and high efficiency", *Turkish Journal of Electrical Engineering & Computer Sciences*, Vol. 22, pp. 1501-1516, doi: 10.3906/elk-1212-143.

Chaouch, S., Hasni, M., Boutaghane, A., Kahla, S., Bacha, S. and Frey, D. (2021), "Novel and simplified model representing current-output phase-shift full-bridge DC-DC LCLC resonant converter in arc welding application", *International Journal of Modelling and Simulation*, Vol. 42 No. 5, pp. 831-854, doi: 10.1080/02286203.2021.1983937.

Cho, J.G., Sabate, J.A., Hua, G.C. and Lee, F.C. (1996), "Zero-voltage and zero-current-switching full bridge PWM converter for high-power applications", *IEEE Transactions on Power Electronics*, Vol. 11 No. 4, pp. 622-628.

Choi, S.W., Lee, J.M. and Lee, J.Y. (2016), "High-efficiency portable welding machine based on full-bridge converter with ISOP-connected single transformer and active snubber", *IEEE Transactions on Industrial Electronics*, Vol. 63 No. 8, pp. 4868-4877.

Demirel, I. and Erkmen, B. (2014), "A very low-profile dual output LLC resonant converter for LCD/LED TV applications", *IEEE Transactions on Power Electronics*, Vol. 29 No. 7, pp. 3514-3524.

Duerbaum, T. (1998), "First harmonic approximation including design constraints", *1998 IEEE 20th International Telecommunications Energy Conference (INTELEC)*, *IEEE, San Francisco, CA*, pp. 321-328.

Ghosh, P.K. (2017), "Pulse current gas metal arc welding characteristics", *Control and Applications*, Springer Nature, Singapore, pp. 303-312, doi: 10.1007/978-981-10-3557-9.

Hallworth, M., Potter, B.A. and Shirsavar, S.A. (2013), "Analytical calculation of resonant inductance for zero voltage switching in phase-shifted full-bridge converters", *IET Power Electronics*, Vol. 6 No. 3, pp. 523-534, doi: 10.1049/iet-pel.2012.0461.

Ji, J.P., Chen, W.J., Yang, X. and Lu, J.J. (2017), "Delay and decoupling analysis of a digital active EMI filter used in arc welding inverter", *IEEE Transactions on Power Electronics*, Vol. 33 No. 8, pp. 6710-6722.

Kar, A., Ghosh, K., Sengupta, M. and Barman, B. (2021), "Analysis and design of efficient sic-based load-resonant converter with advanced features for arc welding applications", *Sadhana-Academy Proceedings in Engineering Sciences*, Vol. 46 No. 4, pp. 1-5, doi: 10.1007/s12046-021-01714-0.

Khoshsaadat, A., Khoshooei, A. and Mohammadi, M. (2020), "Analysis and design of a new current-source output load resonant converter with high capability in line and load regulation", *IEEE Transactions on Circuits and Systems I: Regular Papers*, Vol. 67 No. 8, pp. 2849-2858.

Li, Y., Zhang, K. and Yang, S.F. (2019), "Multimode hybrid control strategy of LLC resonant converter in applications with wide input voltage range", *Journal of Power Electronics*, Vol. 19 No. 1, pp. 201-210, doi: 10.6113/JPE.2019.19.1.201.

Li, Z.Z., Wu, T.W., Zhang, G.D. and Yang, R. (2018), "Hybrid modulation method combining variable frequency and double phase-shift for a 10 kW LLC resonant converter", *IET Power Electronics*, Vol. 11 No. 13, pp. 2161-2169, doi: 10.1049/iet-pel.2018.5304.

Mishima, T., Mizutani, H. and Nakaoka, M. (2017), "A sensitivity-improved PFM LLC resonant full-bridge dc-dc converter with LC antiresonant circuitry", *IEEE Transactions on Industrial Electronics*, Vol. 32 No. 1, pp. 310-324.

Mvola, B., Kah, P. and Layus, P. (2018), "Review of current waveform control effects on weld geometry in gas metal arc welding process", *The International Journal of Advanced Manufacturing Technology*, Vol. 96 Nos 9/12, pp. 4243-4265, doi: 10.1007/s00170-018-1879-z.

Narli, J., Tafti, H.D., Farivar, G.G., Pou, J. and Nguyen, B.X. (2019), "Control scheme for LLC resonant converter with improved performance under light loads and wide input-output voltage variation", *2019 IEEE 11th Energy Conversion Congress and Exposition (ECCE)*, IEEE, Baltimore, MD, pp. 1605-1608.

Narula, S., Singh, B. and Bhuvaneshwari, G. (2016a), "Interleaved CSC converter-based power factor corrected switched mode power supply for arc welding", *IET Power Electronics*, Vol. 9 No. 12, pp. 2404-2415, doi: 10.1049/iet-pel.2015.0510.

Narula, S., Singh, B. and Bhuvaneswari, G. (2016b), "Improved power-quality-based welding power supply with overcurrent handling capability", *IEEE Transactions on Power Electronics*, Vol. 31 No. 4, pp. 2850-2859.

Palani, P.K. and Murugan, N. (2006), "Selection of parameters of pulsed current gas metal arc welding", *Journal of Materials Processing Technology*, Vol. 172 No. 1, pp. 1-10, doi: 10.1016/j.jmatprotec.2005.07.013.

Pang, Q.L. and Zhang, M. (2010), "Design of digital control system for pulsed MIG welding power source", *2010 IEEE 8th World Congress on Intelligent Control and Automation (WCICA)*, IEEE, Jinan, pp. 2492-2495.

Praveen, P., Yarlagadda, P. and Kang, M.J. (2005), "Advancements in pulse gas metal arc welding", *Journal of Materials Processing Technology*, Vols 164/165, pp. 1113-1119, doi: 10.1016/j.jmatprotec.2005.02.100.

Rossi, M.L., Ponomarev, V. and Scotti, A. (2016), "Heat exchange and voltage drop in welding arc column", *IEEE Transactions on Plasma Science*, Vol. 44 No. 10, pp. 2446-2454.

Ruan, X.B. and Yan, Y.G. (2001), "A novel zero-voltage and zero-current-switching PWM full-bridge converter using two diodes in series with the lagging leg", *IEEE Transactions on Industrial Electronics*, Vol. 48 No. 4, pp. 777-785.

Shin, J.Y., Lee, J.M., Choi, S.W. and Lee, J.Y. (2016), "Development of converter for high frequency welding machines using active snubber", *The Transactions of the Korean Institute of Power Electronics*, Vol. 21 No. 4, pp. 351-355, doi: 10.6113/TKPE.2016.21.4.351.

Tayebi, S.M., Chen, X. and Batarseh, I. (2020), "Control design of a dual-input LLC converter for PV-battery applications", *2020 IEEE 35th Applied Power Electronics Conference and Exposition (APEC)*, IEEE, New Orleans, LA, pp. 917-921.

Tran, D., Vu, H.N., Yu, S. and Choi, W. (2018), "A novel soft-switching full bridge converter with a combination of a secondary switch and a non-dissipative snubber", *IEEE Transactions on Power Electronics*, Vol. 33 No. 2, pp. 1440-1452.

Vu, H.N. and Choi, W.J. (2018), "A novel dual full-bridge LLC resonant converter for CC and CV charges of batteries for electric vehicles", *IEEE Transactions on Industrial Electronics*, Vol. 65 No. 3, pp. 2212-2225.

Wang, J.M. and Wu, S.T. (2015), "A novel inverter for arc welding machines", *IEEE Transactions on Industrial Electronics*, Vol. 62 No. 3, pp. 1431-1439.

Wang, J.M., Wu, S.T. and Yen, S.C. (2011), "A simple inverter for arc-welding machines with current doubler rectifier", *IEEE Transactions on Industrial Electronics*, Vol. 58 No. 11, pp. 5278-5281.

Wang, Z.M., Fan, W.Y., Xie, F.X. and Ye, C.X. (2019), "An 8kW LLC resonant converter in plasma power supply based on sic power devices for efficiency improvement", *Circuit World*, Vol. 45 No. 4, pp. 181-188.

Watanabe, T. and Kurokawa, F. (2015), "Efficiency comparison between phase shift and LLC converters as power supply for information and communication equipments", *2015 IEEE 37th International Telecommunications Energy Conference (INTELEC)*, IEEE, Osaka, pp. 1-5.

Wu, H., Zhan, X. and Xing, Y. (2017), "Interleaved LLC resonant converter with hybrid rectifier and variable-frequency plus phase-shift control for wide output voltage range applications", *IEEE Transactions on Industrial Electronics*, Vol. 32 No. 6, pp. 4246-4257.

Wu, K.Y., Wang, Y.F., Cao, X.W., Zhan, J.T., Hong, X.B. and Yin, T. (2021), "GMAW power supply based on parallel full-bridge LLC resonant converter", *International Journal of Electronics*, pp. 1-23, doi: 10.1080/00207217.2021.2001872.

Yang, B. (2003), "Topology investigation for front end DC/DC power conversion for distributed power system", [online] Virginia tech center for power electronics systems, available at: https://cpes.vt.edu/library/viewabstract/3985 (accessed 24 February 2022).

Yang, B., Lee, F.C., Zhang, A.J. and Huang, G.S. (2002), "LLC resonant converter for front end DC/DC conversion", *2002 IEEE 17th Applied Power Electronics Conference and Exposition (APEC)*, IEEE, Dallas, TX, pp. 1108-1112.

Yun, D.H., Lee, W.S. and Lee, J.Y. (2021), "A 3-leg inverter-based high-frequency welding power supply capable of AC 220 and 440 V operation", *IEEE Transactions on Power Electronics*, Vol. 36 No. 11, pp. 12877-12888.

Corresponding author

Kaiyuan Wu can be contacted at: wuky@scut.edu.cn